

ALBERT-LUDWIGS-UNIVERSITÄT FREIBURG

MASTER THESIS

---

# Readout of Wavelength-shifting Optical Modules

---

*Author:*

Johannes ALT

*Supervisor:*

Prof. Dr. Horst FISCHER

February 8, 2023



*Fakultät für Mathematik und Physik*

---



## **Abstract**

todo



## **Zusammenfassung**

todo



# Contents

<b>1</b>	<b>Introduction</b>	<b>3</b>
<b>2</b>	<b>One Cell Prototype</b>	<b>7</b>
2.1	The Cell & Liquid Scintillator . . . . .	7
2.2	Wavelengthshifting Optical Module & Optical Coupling . . . . .	9
2.3	Silicon Photomultiplier . . . . .	10
2.4	The eMUSIC board . . . . .	13
2.5	The GANDALF Module . . . . .	19
2.5.1	Input Mezzanine Cards . . . . .	19
2.5.2	GIMLI Mezzanine Cards . . . . .	21
2.5.3	Usage of the GANDALF with Silicon Photomultipliers (SiPMs)	22
<b>3</b>	<b>Setup</b>	<b>24</b>
<b>4</b>	<b>Results of the Data Acquisition (DAQ) tests</b>	<b>25</b>
4.1	Input offset voltage . . . . .	25
4.2	Pole-zero cancellation . . . . .	26
4.3	High and low transimpedance and lower attenuation . . . . .	29
4.4	Dark count measurements . . . . .	29

<b>5 DAQ performance at the Deutsches Electronen SYnchrotron (DESY) testbeam</b>	<b>30</b>
<b>6 Summary and Outlook</b>	<b>31</b>
<b>A List of acronyms</b>	<b>32</b>
<b>List of Figures</b>	<b>34</b>
<b>List of Tables</b>	<b>35</b>
<b>Bibliography</b>	<b>36</b>

# Chapter 1

## Introduction

So far, the best physical description of the universe is provided by the Standard Model (SM). However, through observations of different phenomena, which the SM can not explain, like neutrino oscillation [1] and the rotation velocity in galaxies [2], it is known that the SM can not be a complete theory [3]. Therefore different experiments are in development or are operating to search for new physics and particles outside the SM. One possible future experiment to join the search for new physics is the proposed Search for Hidden Particles (SHiP) experiment. It is an intensity frontier experiment using the 400 GeV proton beam from CERN’s Super Proton Synchrotron (SPS) and dumping it into a fixed target in order to observe rare events. SHiP is planned to be a zero background experiment to detect these rare events. It searches for long-lived heavy particles from the so-called Hidden Sector (HS), for example, heavy right-handed leptons, dark photons, and light dark matter [4].

?? shows the overall structure of SHiP. The 400 GeV protons get dumped into a high-density target, for example, a target out of tungsten. Through the interaction between the protons and the target, SM particles and HS particles can be produced. In order to remove the SM particles, two shieldings are used. The first one is a hadron absorber which is placed behind the target to absorb produced hadrons and electrons. Afterward, the muon shield utilizes magnetic fields to deflect the produced muons out of the beamline. So only neutrinos and HS particles remain. Behind the muon shield is a neutrino and scattering detector for secondary science cases. The

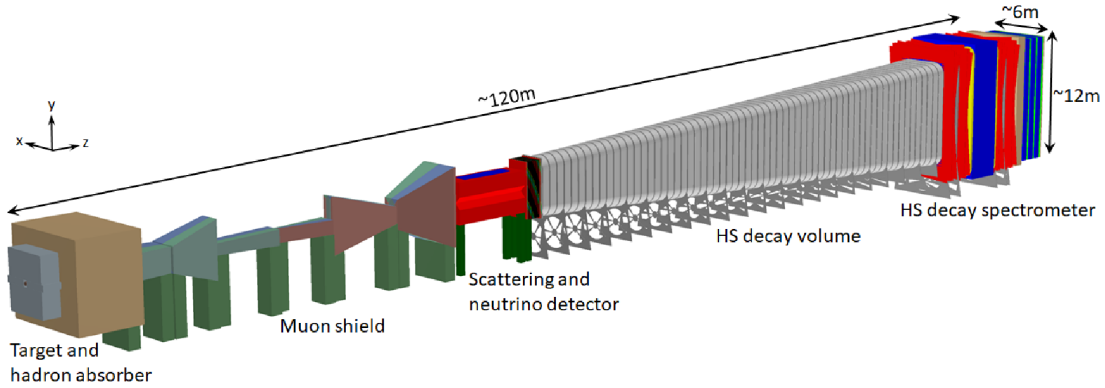


Figure 1.1: Overview of the proposed setup for the SHiP experiment. The target on the left is used as a beam dump for the SPS. Most SM particles get absorbed by the hadron absorber directly behind the target. A magnetic muon shield deflects the muon, which will not be absorbed by the hadron absorber, away from the beam line. After the muon shield is a scattering and neutrino detector, and afterward, the 50 m long decay volume in which non SM particles created at the target can decay into SM particles. Behind the decay volume, the decay spectrometer is placed. To achieve the zero background goal, the Surround Background Tagger is around the decay volume. [3]

next part is the HS decay volume. It is a 50 m long vacuum chamber in which the HS particles can decay into SM particles. The decay products then get detected in the decay spectrometer behind the HS decay volume. With the data produced by the decay spectrometer, the events can get reconstructed.

One problem for the measurement is SM particles entering the decay volume and getting falsely reconstructed as HS events in the spectrometer. An example of such a background is muons deflected by the muon shield and reflected at the walls of the facility into the decay volume, mimicking the decay products of an HS event in the spectrometer. Therefore it is crucial for the zero background requirement to detect the particles entering the decay volume and tag every event that could be caused by the entering particle as background. This task is meant to be done by the Surrounding Background Tagger (SBT). As the name suggests, it surrounds the HS decay volume, detecting particles entering it. It is currently in development and this thesis is part of the R&D effort toward it. In the following, the SBT and the principles of the different parts are described. The details of the different parts important for this thesis are presented in more detail in the next chapter.

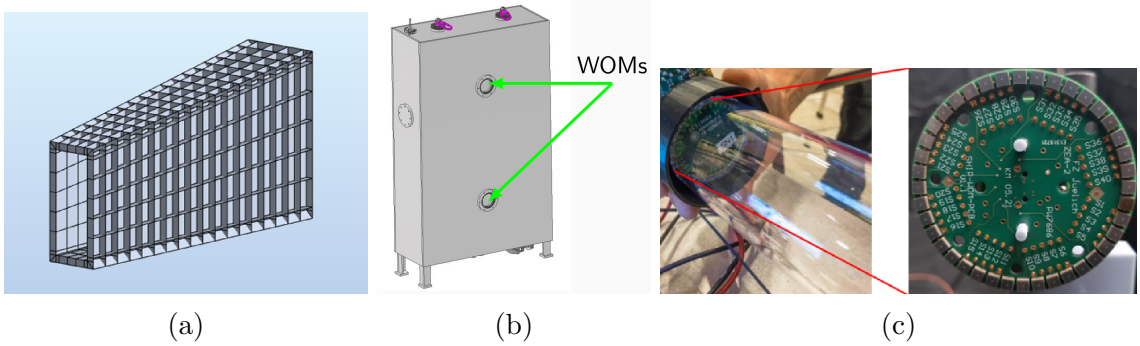


Figure 1.2: The structure of the Surrounding Background Tagger (SBT). Left is the SBT with approximately 2000 cells [1]. Then the prototype of one example cell is shown in b) [1]. The light produced by the liquid scintillator inside the cells is captured by two Wavelengthshifting Optical Modules (WOMs) per cell, an example is shown in c) [1], and then guided to an array of Silicon Photomultiplier which will detect the light.

To make the tagging of background events possible and efficient and avoid the incorrect tagging of many HS events different pieces of information need to be known about the particles entering the decay volume. These pieces of information are the energy of the entering particles, the time at which they are entering the decay volume, and the space coordinates at which they are entering. Therefore the SBT is designed as a five-dimensional tagger. It will consist of approximately 2000 cells that form the walls on the side as well as the top and bottom of the vacuum decay chamber. The structure is shown in ???. In order to fit the overall truncated pyramid shape of the decay volume, the cells have an unsymmetric shape, an example is shown in ???. Both of the long edges are parallel, but the shorter sides are not. The depth of the cells is 20 cm and the wall thickness is planned to be 2 cm [1]. For the detection of particles, a liquid scintillator will be filled into the cells. A particle passing through one or more cells will deposit energy in the scintillator, causing the emittance of scintillation light. The amount of emitted light is correlated to the amount of energy deposited in the scintillator. Two Wavelengthshifting Optical Modules (WOMs), PMMA tubes coated with wavelengthshifting paint, are placed in each cell to collect the scintillation light and guide it to an array of SiPMs. The signals from the SiPMs can be amplified, digitized, and further processed. Both a WOM and a SiPM array are shown in ??.

This thesis is in the scope of the R&D of the SBT. For the R&D of the SBT, a prototype of one of the cells was built, with which important parts can be tested. Starting from the cell's material itself, a reflecting coating on the inside of the cell, the coated WOMs, and the SiPMs, to name a few. This thesis is about the readout of the WOMs of the prototype. Since the Application Specific Integrated Circuit (ASIC) meant to be used for the readout in the SBT is in development by the Forschungszentrum Jülich and not yet finished, another readout is needed for the One Cell Prototype in order to test it. The next chapter presents the One Cell Prototype with a focus on the WOM readout.

# Chapter 2

## One Cell Prototype

The work presented in this thesis is done in the framework of the One Cell Prototype. Therefore the prototype is described in more detail in this chapter. Although the important parts of the One Cell Prototype are all mentioned here, the main focus lies on the amplifier and the digitizer since these are the most relevant parts of this thesis. Firstly the cell and the liquid scintillator are shown, followed by the WOM used to capture the scintillation light, the SiPMs used for the light detection, and the optical coupling between the WOM and the SiPMs, are presented afterward. Subsequently, the amplifier and the digitizer are introduced.

### 2.1 The Cell & Liquid Scintillator

In ??, the One Cell Prototype is shown. It is 80 cm wide and around 120 cm high. However, the precise height depends on the position in the cell due to the asymmetric shape. The walls of the cell consist of 1 cm thick corten steel. The steel was chosen because of the rather low price tag, which is an important aspect considering the size of the SBT. A thickness of 1 cm is only half of the planned 2 cm wall thickness of the SBT design. The SBT needs such thick walls in order to withstand the vacuum on the inside. For the R&D with the One Cell Prototype, the thickness was reduced to be able to perform measurements with different wall thicknesses by adding steel plates to the outside. This is important in case the SBT design changes, for example



Figure 2.1: The One Cell Prototype at the DESY testbeam area a) and a PMMA vessel with a Wavelengthshifting Optical Module inserted and a SiPM board attached b). []

by replacing the vacuum with helium. One side of the cell has two holes with a cm radius. They have an equal distance to both side walls. The lower hole is 30 cm away from the bottom of the cell, and the upper hole is 30 cm below the top. In each of these holes, a PMMA vessel, shown in ??, is placed to house the two WOMs and protect their wavelengthshifting coating from the liquid scintillator. A reflective paint was applied to the inside of the cell to increase the scintillator's light yield and therefore increase the detector's efficiency.

The cell is filled with the liquid scintillator Linear Alkyl Benzene (LAB) mixed with  $2 \frac{g}{L}$  Diphenyloxazole (PPO) in order to allow decompression and compression by temperature change, an expansion vessel is mounted on top of the cell. The cell was overfilled with scintillator, in order to still being full if the temperature declines and the scintillator compresses. Gaseous nitrogen fills out the remaining volume of the expansion vessel to serve as a compressible volume.

LABs emission spectrum is shown in ?? . Most of the scintillation light has a wave-

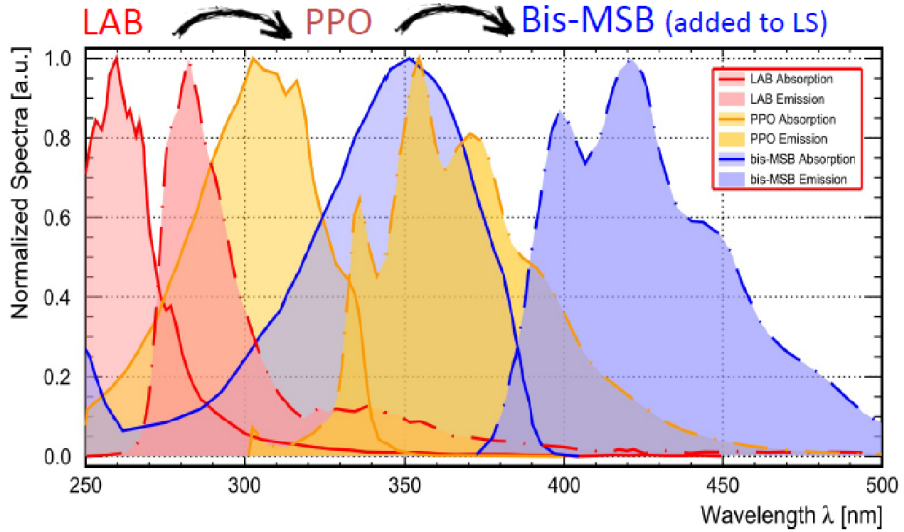


Figure 2.2: The emission spectrum of the liquid scintillator components LAB and Diphenyloxazole (PPO) and the wavelength shifter Bis-MSB. []

length of 320 nm to 360 nm. In order to capture the light and to shift the wavelength towards values for which the used SiPMs have a higher detection efficiency, WOMs are used. In the next section, these WOMs and the optical coupling between them and the SiPMs are presented.

## 2.2 Wavelengthshifting Optical Module & Optical Coupling

So-called WOMs are used to capture the scintillation light. They are PMMA cylinder walls with a 6 cm outer diameter and a 3 mm wall thickness. The design and material choice both make the cost of the light collection relatively cheap. Both the inside and outside of the PMMA cylinder are coated with the wavelength shifter Bis-MSB []. So the captured photons are shifted to a higher wavelength, for which the SiPMs used for the light detection have a higher efficiency. ?? shows the wavelength spectrum of the wavelength-shifted light. The photons which enter the WOM are trapped there by total reflection on the walls. They can leave the WOM at its end, where an array of forty SiPMs can detect them. For a good optical coupling between the WOM and the SiPMs, either optical grease or silicon pads can be used.

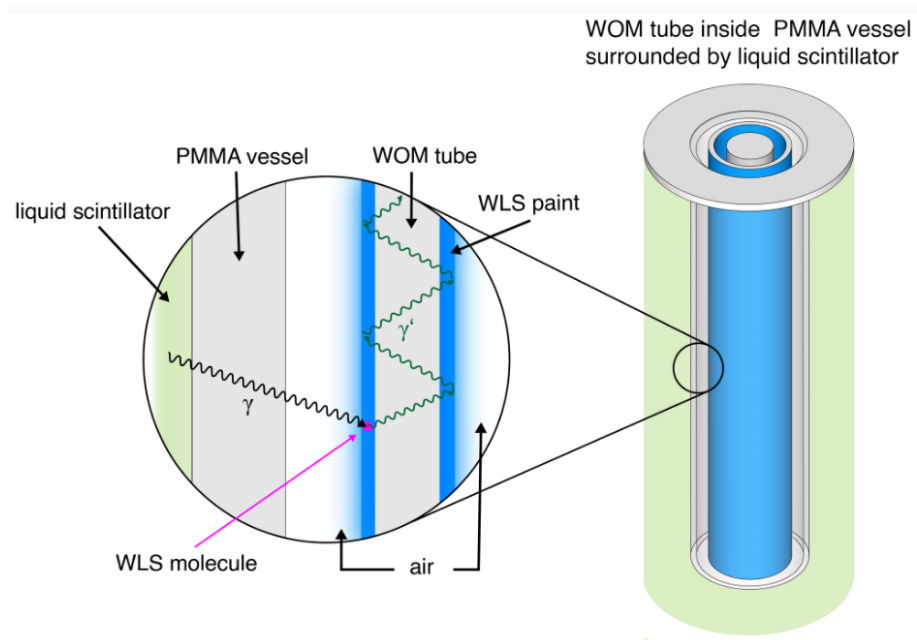


Figure 2.3: A Wavelengthshifting Optical Module (WOM) is a PMMA tube coated with the wavelength shifter Bis-MSB. If a photon in the UV range hits the WOM, its wavelength gets shifted. Afterward, in the WOM, the photon is trapped by total reflection. At the end of the WOM, the photon can be detected by a photosensor. [?, ]

?? illustrates the principle of the WOM with the wavelength shifting and capture by total reflection.

In the next part, the SiPMs, which detect the light captured by the WOMs, are presented.

## 2.3 Silicon Photomultiplier

In order to correctly identify and tag background events, the light detection of the SBT has to provide accurate timing information. Furthermore, due to the number of cells and WOMs in the SBT, it should not cost a lot per WOM. To fulfill both requirements, SiPMs were chosen as photodetectors. These photodetectors consist of up to thousands of pixels. Each pixel is a photodiode with a typical edge length between  $10\text{ }\mu\text{m}$  and  $100\text{ }\mu\text{m}$  [5]. If triggered by light, a SiPM sends out a charge

signal proportional to the number of triggered pixels. In the case that the number of incoming photons is low compared to the number of pixels, such that two photons hitting the same pixel is unlikely, the charge signal is linear to the light intensity. The charge signal possesses a fast-rising edge with a rise time of the order of tens of s [5]. Besides the excellent time resolution, SiPMs also make it possible to count the arriving photos with a sensitivity down to single photons [6].

Each pixel in the SiPM is an Single Photon Avalanche Diode (SPAD), which is a Avalanche Photodiode (APD) supplied with a voltage greater than its breakdown voltage. In the following, the principle of such an APD and SPAD are explained.

Similar to every photodiode, APD utilize, the photoelectric effect to generate an electric charge signal in response to a light signal. They consist of doped silicon. An example is shown in ?? . It has a strongly n-doped layer, followed by a strongly p-doped layer, an intrinsic, weakly p-doped layer, and another p-doped layer. By adding the intrinsic layer, the region in which the photons can be absorbed increases. If a photon gets absorbed, it generates an electron-hole pair. When a reversed bias voltage is applied, the electric field in the APD separates the *eh*-pair. In case the APD is operated in the Geiger mode, meaning the bias voltage is higher than the breakdown voltage of the APD, the electric field at the strongly doped *p*- and *n*-layer is sufficiently high, that a self-sustaining avalanche is triggered by either the electron or the hole moving through it. Then the APD is called SPAD. The macroscopic signal of a SPAD makes it possible to detect single photons. In order to stop the avalanche, a quenching resistor is connected in series to the SPAD. With an increasing current signal flowing through the quenching resistor, the voltage drop at this resistor increases, and thus the bias voltage at the SPAD decreases. When the bias voltage drops under the breakdown voltage, the avalanche is no longer self-sustaining and stops. Thus the signal amplitude of a SPAD is always similar, independent of how many photons arrive at the same moment.

In SiPMs, hundreds to thousands of SPADs are connected in parallel, each with a high-resistance quenching resistor in series. Usually, the SPAD pixels are placed in a rectangular form with an edge length of a few mm. ?? shows a picture of a SiPM and one picture of a single pixel of a SiPM. Due to the property of the SPADs that the output signal is always similar for each SPAD, the output signal of a SiPM is



Figure 2.4: Composition of an avalanche photodiode with the bias voltage  $V_B$  applied in the reverse direction. Between the contact to the ground and the strongly doped  $n^+$  layer is the quenching resistor  $R_q$  connected in series. Next to the  $n^+$  layer is a strongly doped  $p^+$  layer. In the region of these two layers is the electric field, shown in the right figure, the strongest. There, an electron or hole can initiate an avalanche. After the  $p^+$  layer is an intrinsic weakly doped  $\pi$  layer. This layer increases the sensitive volume of the diode. If an electron-hole pair is created, it gets separated by the electric field. The hole drifts towards the multiplication region and can start an avalanche. The next layer is a  $p^+$  layer, which connects to a metal connector and high voltage. The picture in the middle illustrates the number of donators  $n_D$  and acceptors  $n_A$ , and the last picture illustrates the field strength at the different regions of the APD. []

the output signal of one SPAD multiplicated by the number of triggered SPADs. Therefore, if the number of photons arriving simultaneously at a SiPM is low enough that the probability of one SPAD being hit by two or more photons is low, one can count photons with a SiPM. This and the relatively low cost, high durability, and impassivity to magnetic fields make them a good option for photodetection for the SBT and similar detectors. However, due to the sensitivity down to single photons, also *eh*-pairs created by thermal excitation will cause signals indistinguishable from signals caused by photons. These signals are called Dark Count (DC).

An essential property of a SiPM is the gain  $G$ . It describes the number of charge carriers released in each avalanche. Due to the quenching, this parameter is well-defined [6]. It can be calculated from the applied voltage  $U_{\text{bias}}$ , the breakdown voltage  $U_{\text{bd}}$  and the capacitance  $C_d$  of a SPAD with

$$G = \frac{(V_{\text{bias}} - V_{\text{bd}}) \cdot C_d}{e}. \quad (2.1)$$

Here,  $e$  represents the charge of one electron. Usually, the gain is in the order of  $10^5$  to  $10^7$  [5]. Since the breakdown voltage of different SiPMs of the same model can differ slightly, also the gain with the same bias voltage can differ.

The next section presents the ASIC used to amplify the SiPM signals.

## 2.4 The eMUSIC board

Since the signals of the SiPMs are tiny, they need to be amplified. For this purpose, the enhanced Multiple Use SiPM IC for photodetector readout (eMUSIC) ASIC by Scientifica was chosen, and a custom Printed Circuit Board (PCB) housing the eMUSIC ASIC, from here on called eMUSIC board, was designed by the electrical engineers of the University of Freiburg. In the following first, the ASIC itself and afterward, the eMUSIC board will be presented.

**The eMUSIC ASIC** was developed by Scientifica for the readout of SiPMs. It is mainly an amplifier and a shaper, but it also offers other options like digital trigger signals if the signal crosses an adjustable threshold. The ASIC's block diagram is

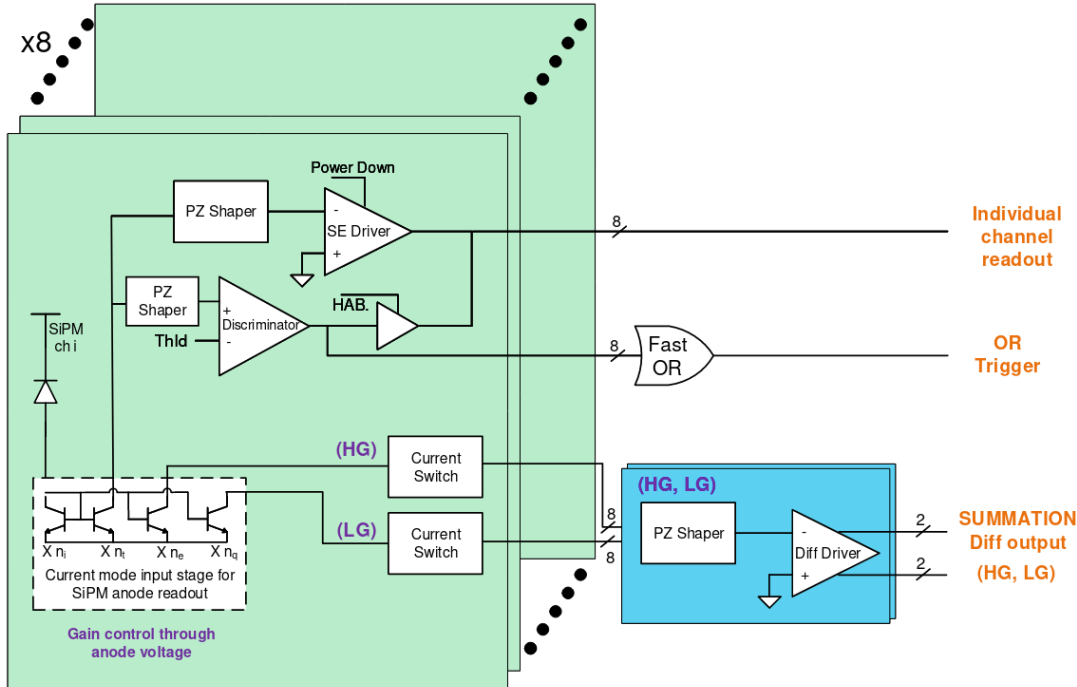


Figure 2.5: The block diagram of the eMUSIC ASIC. At the input is the current mode input stage, which can also set an offset voltage on the input to adjust the overvoltage channel by channel. The signal then gets shaped by the pole-zero cancellation shaper and amplified and can be read out for each channel as a single-ended signal. The discriminator can set a threshold to create a digital signal which can be read out channel by channel instead of the analog output signal. A fast OR output can also be used to put out a digital OR of all eight discriminator outputs. With the summation outputs, one can put out the sum of an arbitrary set of channels with two gains as differential signals. [?]

shown in ???. It has eight input channels, each equipped with a  $\approx 1\text{ V}$  anode voltage control to equalize the applied overvoltage between the different channels. Because the SiPMs deliver a charge signal, each channel has a current mode input stage. The eMUSIC ASIC was designed to have a low input transimpedance but provides the option of a high transimpedance mode with which the gain can be increased. Each individual channel has a bandwidth of 150 MHz and a pole-zero cancellation, schematics shown in ??, with two adjustable resistors and an adjustable capacitor. It can be used to decrease the Full Width at Half Maximum (FWHM) of the output signal to below 10 ns. But a smaller width also attenuates the amplitude of the signal.

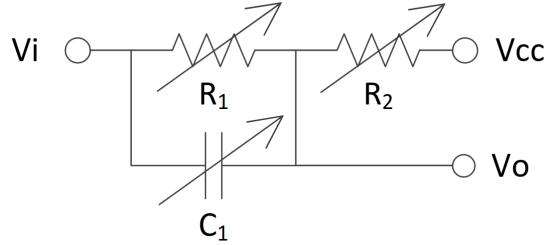


Figure 2.6: Sketch of a pole-zero cancellation with adjustable resistors and capacitor, the input voltage  $V_i$ , the output voltage  $V_o$ , and the operation voltage  $V_{cc}$ . [?]

The resistor has eight possible values it can be set to, and the capacitor has thirty-two different steps. Although the eMUSIC provides the option of a lower attenuation mode of the pole-zero cancellation, a compromise between smaller signal width and higher amplitude should be chosen depending on one's needs. Alternatively, the pole-zero cancellation can be disabled completely, resulting in the highest signal amplitude possible with the eMUSIC but also in the longest signal. The signal after the shaper can be put out with an analog output for each channel.

Each channel also possesses a discriminator with an adjustable threshold to create a channel-by-channel trigger signal. These logical signals can be either put out by using the individual output of the channel for the digital signal instead of the analog waveform or by using the fast OR of all channels. This fast OR allows, for example, the external triggering of the digitizer, which then digitizes the analog waveforms if the waveform of one or more channels surpasses the threshold. The dynamic range of the output for the single-ended signals is 1 V if the load on the output is  $50\Omega$  and 2 V if a high impedance load is used on the output. Using the low transimpedance mode, the gain of the single-ended output is  $180\Omega$ , and with the high transimpedance mode, it is  $480\Omega$ . Over the first half of the dynamic range, the response of the eMUSIC is linear, and over the second half, it is non-linear.

Besides the individual readout of the eight channels, the eMUSIC can sum up the signal of an arbitrary set of channels with both high and low gain and put them out via two differential outputs. The bandwidth of this summation output is 500 MHz, and the output range is 1.25 V. Depending on whether the high or low transimpedance is used, the gain of the high gain summation is  $690\Omega$  or  $90\Omega$  and  $315\Omega$  or  $45\Omega$  for

the low gain summation. The response of the summation output is linear over the dynamic range.

Besides choosing the channels for summation, also each of the eight single-ended outputs can be individually turned on and off. Another important option that can be configured is the adjustment of the output DC offset to maximize the rail-to-rail voltage swing.

The trigger threshold for the digital outputs can be set with two parameters. The first one is the bandgap voltage  $V_{bg}$  of the comparators, which can be adjusted in eight steps between 487.22 mV and 2436.8 mV. The second parameter sets the Digital to Analog Converter (DAC) value  $N_{DAC}$  for the comparators. It can be set to DAC counts from 0 to 511. The finer threshold steps  $V_{fine}$  can be calculated with

$$V_{fine} = 1637.79 \text{ mV} - N_{DAC} \cdot 3.1445 \text{ mV}. \quad (2.2)$$

With  $V_{bg}$  and of  $V_{fine}$  or  $N_{DAC}$ , the final threshold

$$V_{th} = 1.5 \cdot V_{bg} - 0.5 \cdot V_{fine} \quad (2.3)$$

$$= 1.5 \cdot V_{bg} - 0.5 \cdot (1637.79 \text{ mV} - N_{DAC} \cdot 3.1445 \text{ mV}) \quad (2.4)$$

can be calculated.

**The eMUSIC board** was designed at the University of Freiburg. A graphic of the board is shown in ???. Its heart is the eMUSIC ASIC (U1). In order to program the ASIC, the ATmega328P-AU microchip (U4) is placed on the board. The microchip can be programmed with the XXXX software by XXXXX and the XXXXX, which is connected to the computer via USB and can be plugged into the J4 connector on the eMUSIC board. After programming the microchip, it only has to be programmed again if the reset button SW1 is pressed. Then the eMUSIC ASIC can be configured by using a TTL-to-USB adapter connected to a computer and the P3 connector, and the software of the minimusic board. The minimusic board is a commercial product using the eMUSIC ASIC. Due to the eMUSIC board being designed to work with the minimusic software, one avoids the need to write software and also has the security that the used software was tested and is working

correctly. Two functions of the minimusic software are not usable on the eMUSIC board, the calibration of the threshold and the calibration of the DC offset on the outputs. Therefore these two need to be set by the user.

The high voltage for the SiPMs can be supplied via the P2 SMA connector. On the backside of the PCB is an LSHM-150-XX.-XXX-DV-AN-XX connector located to connect the board to the SiPM board. Via this connector, the high voltage is brought to the SiPMs, and the signals are brought to the eMUSIC inputs. The eight single-ended outputs can be read out by the SMA connectors K1 to K8. The fast OR signal can be read out via the K9 connector. Both the high and low gain differential summation outputs are connected to the pins of the J6 connector.

The board also provides the possibility via the P1 connector to power the six LEDs soldered onto the SiPM boards. However, the usage of this is not advised since this will introduce interferences into the signals.

The amplified single-ended output signals then can be digitized. For this task, the GANDALF module was chosen, which is described in the next section.

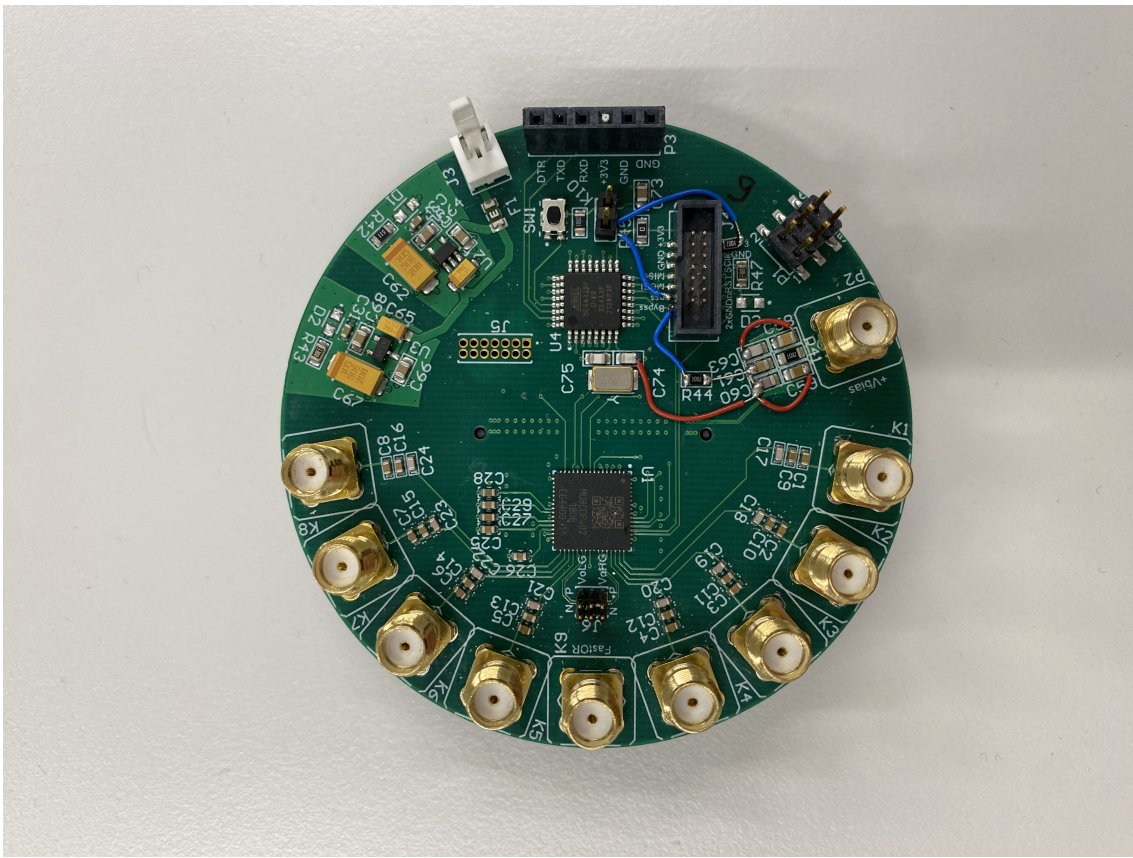


Figure 2.7: Picture of the eMUSIC board with the eMUSIC ASIC, the eight single-ended channel-by-channel SMA signal outputs, the SMA fast OR output, the differential signal output, the SMA connector for the high voltage supply of the SiPMs, and the connectors to program and power the board.

## 2.5 The GANDALF Module

The amplified and shaped output signal of the eMUSIC ASIC needs to be digitized. This step is done by GANDALF modules. Originally developed at the University of Freiburg for the Common Muon Proton Apparatus for Structure and Spectroscopy (COMPASS) experiment, it has a modular design to fill different roles in the experiments DAQ. Using mezzanine cards, different signal, clock, and trigger inputs can be chosen. In the following, the GANDALF module will be introduced. The mezzanine cards not used in this work are therefore only mentioned but not presented in detail. An overview of a GANDALF module is shown in ??.

### 2.5.1 Input Mezzanine Cards

The GANDALF module has two mezzanine card slots for input signals. For these slots, three different mezzanine cards were developed, Analoge Mezzanine Card (AMC), Digital Mezzanine Card (DMC), and Optical Mezzanine Card (OMC). First, the last two mezzanine cards are shortly presented for completeness but are not relevant to the work done in this thesis.

**The DMC** has 64 digital inputs. Using either the LVDS or the LVPECL signal standard, one can use the DSP-Field Programmable Gate Array (FPGA) logic for tasks like trigger decisions, time-to-digital conversion, or pattern generators, to name a few. By changing the direction of the input buffer on the DMC PCB, the 64 channels of the DMC can be used as outputs instead of inputs.

**The OMC** has four 3.25 Gs transceivers to receive digital information, which can be further processed by the DSP-FPGA. With this mezzanine card, the GANDALF can be used, for example, to merge data or as a concentrator.

**The AMC** is designed to digitize analog input signals. For digitization, eight Analog to Digital Converter (ADC) are used. There are AMC with two different ADC available. One is the *ADS5463*, with 12 and up to 500  $\frac{\text{MS}}{\text{s}}$ , and the other is

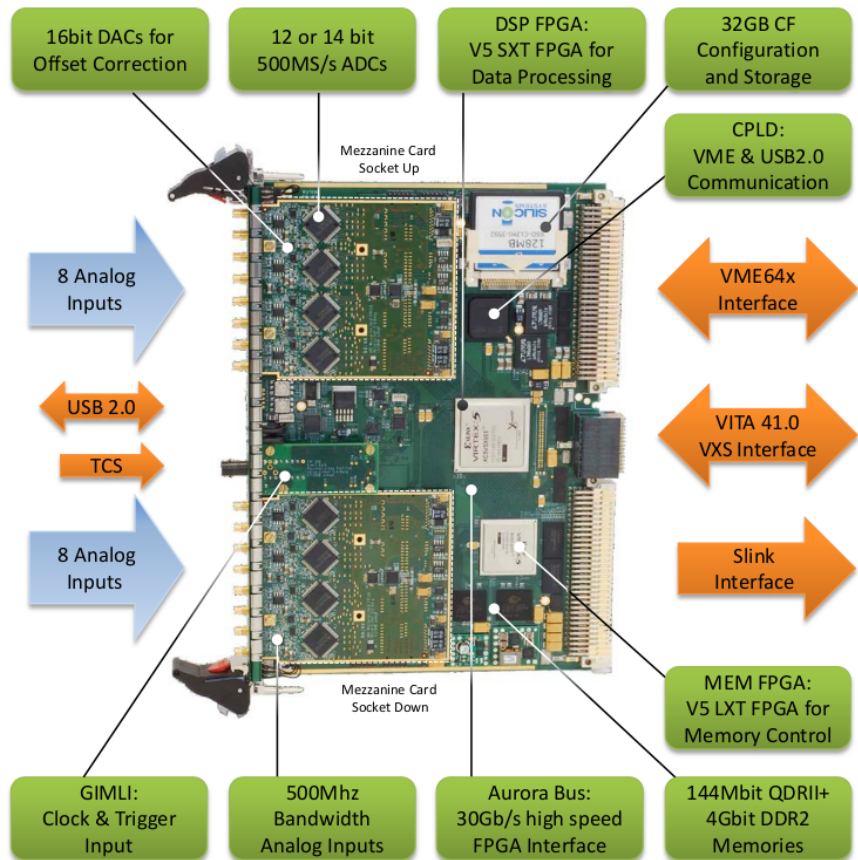


Figure 2.8: Overview of the GANDALF module equipped with Analog Mezzanine Cards (AMCs) and the fiber Gimli mezzanine card for clock and trigger input. The analog waveforms are digitized by the AMCs, and the digitized data is processed by the DSP FPGA. The MEM FPGA handles the memory of the processed data, which can be transferred to a computer via the USB interface on the front of the VME or S-Link interfaces on the backplane. [?]

the *ADS5474* which samples with up to  $400 \frac{\text{MS}}{\text{s}}$  at 14. The Effective Number of Bits (ENOB) of both ADCs are 10.4 and 11.2, respectively. Each AMC has eight SMC connectors for the inputs. There are AMC operating in *normal mode*, meaning each SMC connector is connected to one ADC, resulting in eight channels with up to  $500 \frac{\text{MS}}{\text{s}}$  or  $400 \frac{\text{MS}}{\text{s}}$  per AMC. In order to increase the sampling frequency, AMCs which operate in the *interleaved mode* were built. On these AMCs, four inputs are connected to two ADCs each, and therefore every second SMC connector is a dead end. The clock signals which provide the sample tact for the two ADCs of one channel have  $180^\circ$  phase offset with respect to each other. By this, the sampling frequency is doubled to up to  $1 \frac{\text{GS}}{\text{s}}$  or  $800 \frac{\text{MS}}{\text{s}}$ , but the number of channels per AMC is reduced from eight to four. The dynamic input range of the AMC is 4.4 and can be shifted from the negative unipolar range  $-4.4\text{ V}$  to  $0\text{ V}$  up to the bipolar range  $-2.2\text{ V}$  to  $2.2\text{ V}$ . This shifting is done by an *AD5665R*, a 16 DAC. The dynamic range was chosen because in the COMPASS experiment, for which the GANDALF was developed, negative voltage pulses created by Photomultiplier tubes (PMTs) needed to be digitized. However, because the used ADCs expect positive differential signals, inverting operational amplifiers are used to change the polarity of the signal. By changing the gain of the amplifiers, one can decrease the input range and therefore increase the amplitude resolution. The AMCs used in this thesis are 12 AMCs in the *interleaved mode* and a dynamic range of 2.2.

### 2.5.2 GIMLI Mezzanine Cards

The third mezzanine card slot is for the GIMLI mezzanine cards, which are responsible for the clock and external trigger signals. For this mezzanine card, three different options were developed. One GIMLI card, which takes the clock and trigger from the backplane, if one wants to use the create to distribute the signals. The fiber GIMLI has one fiber input to receive the clock and trigger via optical fiber. And the copper GIMLI, which was used for this work and is presented in the following.

The copper GIMLI, shown in ??, provides the option to use an external or an internal clock. If only one GANDALF module is used, the internal 20 MHz clock of the copper GIMLI can be used. It is provided by an onboard oven-controlled oscillator (OCXO) with a jitter of less than 2.3 ps. In case two or more GANDALFs are

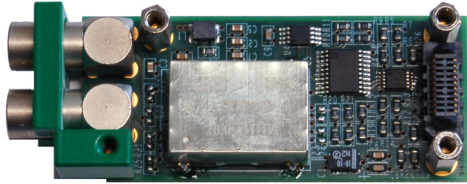


Figure 2.9: Picture of the copper GIMLI with an internal 20 MHz clock generated by an onboard oven-controlled oscillator. With the LEMO connectors external clock and trigger NIM signals can be provided for the GANDALF. [?]

used, an external clock is required to ensure a synchronized clock on all GANDALF modules. For this case, the copper GIMLI has a LEMO connector as input for an external clock with Nuclear Instrumentation Module (NIM) signal standard. Via a second LEMO connector, an external NIM trigger signal can be connected to the GANDALF module.

### 2.5.3 Usage of the GANDALF with SiPMs

In this work, the GANDALF was used for digitizing the output signal of the eMUSIC ASIC. As mentioned above in ??, these signals have a positive polarity. But because the GANDALF was designed for the digitization and processing of negative voltage pulses created by a PMT, this caused some problems. Since after the inverting operational amplifiers in the GANDALF, the SiPM signals have a negative polarity, the input voltage range needs to be chosen to be bipolar and around  $-1.1\text{ V}$  to  $1.1\text{ V}$ . Also, the self-trigger of the GANDALF needed to be adjusted. It functions via samples over threshold. The user can set a threshold and a number of consecutive samples which need to be over the threshold for the GANDALF to trigger an event. Since after the inverting of the positive signals, the signals have a negative polarity, and the threshold needs to be set to a lower ADC value than the baseline. In addition to that, the sample over threshold condition in the GANDALF firmware needed to be inverted to trigger if a number of consecutive samples were below the threshold. The new firmware with the inverted trigger condition was tested and worked as intended, with the exception of one bug. If the data rate from the GANDALF to

the DAQ computer exceeds the maximum possible data rate,  $20 \frac{\text{MB}}{\text{s}}$  in the case of the USB interface, incomplete events will be written down to disk. This is most likely caused by a missing VHDL file that was not included in the new firmware and which would, in case the buffer of the GANDALF is completely filled, prevent the GANDALF from sending incomplete events to the computer. For the intended use of this bug should not be a problem since the data rate is expected to be way below the possible  $20 \frac{\text{MB}}{\text{s}}$ .

# Chapter 3

## Setup

# Chapter 4

## Results of the DAQ tests

### 4.1 Input offset voltage

The first measurement is to find out the input offset voltage of the eMUSIC for different DAC values. This needs to be done to find out the exact overvoltage of the SiPMs. In order to perform this measurement, the setup in ?? was assembled. The eMUSIC board was powered by the 8V power supply and the XXXXXXXX power supply was used to supply the high voltage. It was set to 16V since it was unimportant for the high voltage to be over the breakdown voltage of the SiPMs. It should only be over the maximum input offset the eMUSIC can generate for the resulting voltage to be applied in reverse direction to the SiPMs. For this measurement the eMUSICs input DAC settings, which can range from 0 to 511, were set to 0. Then the voltages between the negative high voltage pole and the voltage on the cathode of the SiPMs were measured. This measurement was done for one SiPM of each SiPM group. The chosen SiPM were 1, 6, 11, 16, 21, 26, 31 and 36. After measureing the voltages, the DAC setting was increased in steps of 50 DACu. For each setting the eight voltages were measured again.

The measurement for

## 4.2 Pole-zero cancellation

In this section pole-zero cancellation shaper and its effect with different settings tested. The tests were done using the setup described in ???. For the amplification the eMUSIC board 2 was chosen and the digitization was done by a GANDALF module. The eMUSIC settings of one of these measurements are shown in ?? in the appendix. For the other measurements, the only thing changing in the settings are the pole-zero settings. Each measurement includes XXXXX events, for which the mean value is shown in the plots below. The values for the amplitude and FWHM were calculated for each individual waveform and their mean values are presented here for the different measurements.

First the pole-zero cancellation was disabled to perform measurements for a reference amplitude and FWHM. In ?? the mean of all waveforms, measured in channel 0, is shown. The mean amplitude is

$$V_{amp} = (1 \pm 1) \text{ mV} \quad (4.1)$$

and the FWHM is

$$t_{FWHM} = (1 \pm 1) \text{ ns.} \quad (4.2)$$

Next the measurement with enabled pole-zero cancellation and with fixed settings for its capacitor and varying resistor values. The resistor settings were changed to all possible values, from 0 to 7, and the capacitor setting was kept at 31. ?? presents the mean waveforms for the eight measurements. The determined amplitudes and FWHM and the corresponding decrease in respect to the values without pole-zero cancellation are listed in ???. Of all measurements the one with the resistor setting 0 had the highest mean amplitude with

$$V_{amp,R=0} = (1 \pm 1) \text{ mV} \quad (4.3)$$

which corresponds to a amplitude attenuation of  $(1 \pm 1)\%$ . With these settings a

FWHM of

$$t_{\text{FWHM}, R=0} = (1 \pm 1) \text{ ns} \quad (4.4)$$

was measured, which is  $(1 \pm 1)\%$  of the FWHM measured without pole-zero cancellation.

The measurements with different capacitor settings were performed with the resistor setting of 0. For the different measurements, the capacitor settings were changed to all 32 possible values, from 0 to 31. In ?? the mean values for the maximum amplitude and the FWHM as well as the decrease compared to the values with disabled pole-zero cancellation are listed. The mean waveforms for the measurements with the capacitor settings 0, 5, 10, 15, 20, 25, and 31 are shown in ??.



pictures/pz\_resistor.png

Figure 4.1: Mean waveform for different pz-cancellation resistor values.



pictures/pz\_capacitor.png

Figure 4.2: Mean waveform for different pz-cancellation capacitor values.

### **4.3 High and low transimpedance and lower attenuation**

### **4.4 Dark count measurements**

# **Chapter 5**

## **DAQ performance at the DESY testbeam**

After the performance of the DAQ was tested at the testbeam for one week with particles of known energy and known direction of movement, the long term performance of the one cell prototype and the DAQ needs to be investigated. For this purpose, the one cell prototype is assembled at the University of Freiburg, where it is supposed to be taking continuously data for a year.

# Chapter 6

## Summary and Outlook

# Appendix A

## List of acronyms

**SM** Standard Model

**LHC** Large Hadron Colider

**SHiP** Search for Hidden Particles

**SPS** Super Proton Synchrotron

**SBT** Surrounding Background Tagger

**SiPM** Silicon Photomultiplier

**PCB** Printed Circuit Board

**ASIC** Application Specific Integrated Circuit

**DAC** Digital to Analog Converter

**ADC** Analog to Digital Converter

**APD** Avalanche Photodiode

**DAQ** Data Acquisition

**WOM** Wavelengthshifting Optical Module

**SPAD** Single Photon Avalanche Diode

**DC** Dark Count

**DCR** Dark Count Rate

**FPGA** Field Programmable Gate Array

**DESY** Deutsches Electronen SYnchrotron

**eMUSIC** enhanced Multiple Use SiPM IC for photodetector readout

**PMT** Photomultiplier tube

**AMC** Analoge Mezzanine Card

**OMC** Optical Mezzanine Card

**DMC** Digital Mezzanine Card

**NIM** Nuclear Instrumentation Module

**HS** Hidden Sector

**LAB** Linear Alkyl Benzene

**FWHM** Full Width at Half Maximum

**COMPASS** Common Muon Proton Apparatus for Structure and Spectroscopy

**ENOB** Effective Number of Bits

**PPO** Diphenyloxazole

# List of Figures

1.1	Overview of the SHiP experiment . . . . .	4
1.2	Overview of the Surrounding Background Tagger . . . . .	5
2.1	One Cell Prototype and PMMA vessel . . . . .	8
2.2	LAB emission spectrum . . . . .	9
2.3	Working principle of a WOM . . . . .	10
2.4	Illustration of a APD. . . . .	12
2.5	eMUSIC block diagram . . . . .	14
2.6	eMUSIC pole-zero cancellation . . . . .	15
2.7	eMUSIC Board . . . . .	18
2.8	Overview of the GANDALF module . . . . .	20
2.9	Copper GIMLI . . . . .	22
4.1	Mean waveform for different pz-cancellation resistor values. . . . .	27
4.2	Mean waveform for different pz-cancellation capacitor values. . . . .	28

## List of Tables

# Bibliography

- [1] SHiP - Search for Hidden Particles, <https://ship.web.cern.ch/>, June 2022
- [2] S. Alekhin et al “A facility to search for hidden particles at the CERN SPS: the SHiP physics case”, Rep. Prog. Phys. 79, Oct 2016, <https://doi.org/10.1088/0034-4885/79/12/124201>
- [3] SHiP Collaboration, “SPS Beam Dump Facility - Comprehensive Design Study”, 2020, arXiv:1912.06356
- [4] J. Kemp, “Development of a silicon photomultiplier based scintillator detector for cosmic air showers” Phd thesis, Dez 2020, RWTH Aachen
- [5] F. Acerbi, S. Gundacker, “Understanding and simulating SiPMs”, NIM-A vol. 926, p. 16-35, 2019. doi: 10.1016/j.nima.2018.11.118
- [6] Hamamatsu Photonics, MPPC, [https://www.hamamatsu.com/content/dam/hamamatsu-photonics/sites/documents/99\\_SALES\\_LIBRARY/ssd/mppc\\_kapd9005e.pdf](https://www.hamamatsu.com/content/dam/hamamatsu-photonics/sites/documents/99_SALES_LIBRARY/ssd/mppc_kapd9005e.pdf), date: 20.06.2022
- [7] Hamamatsu S14160-3050HS Datasheet, [https://www.hamamatsu.com/content/dam/hamamatsu-photonics/sites/documents/99\\_SALES\\_LIBRARY/ssd/s14160\\_s14161\\_series\\_kapd1064e.pdf](https://www.hamamatsu.com/content/dam/hamamatsu-photonics/sites/documents/99_SALES_LIBRARY/ssd/s14160_s14161_series_kapd1064e.pdf), date: 05.05.2022